

# Oxidation kinetics of ZrNbO in steam: Differences between the pre- and post-transition stages

M. Tupin, M. Pijolat, F. Valdivieso \*, M. Soustelle

*Laboratoire des Précédés en Milieux Granulaires CNRS UMR 5148, Centre SPIN, Ecole Nationale Supérieure des Mines, 158 Cours Fauriel, 42023 Saint-Etienne cedex 2, France*

Received 28 October 2004; accepted 16 February 2005

## Abstract

The oxidation by water vapour of a zirconium based alloy, a ZrNbO alloy containing 1% of Nb, has been studied between 500 and 550 °C, the water vapour partial pressure ranging in 13–80 h Pa, using isothermal and isobaric thermogravimetry, and calorimetry. During gravimetry experiments, sudden changes (jumps) in temperature or water vapour pressure have also been performed. It comes out that the kinetic behaviour is different before and after the transition, even though the approximations of steady-state and rate-limiting step are justified in both stages: the influence of temperature jumps is greater in pre-transition, whereas the effect of water vapour partial pressure is more pronounced in post-transition (nevertheless, an accelerating effect is also observed before the transition). No influence of hydrogen partial pressure has been observed. Besides, the higher the Nb content in the alloy, the higher the oxidation rate (in pre-transition). A mechanism has been proposed to account for the results obtained in pre-transition, involving the diffusion of adsorbed species in the porous part of the oxide layer as rate-determining step.

The transition is accompanied by a change in the oxidation mechanism: in the post-transition stage, the kinetic curves being linear, the oxidation may be controlled by an interface step, which is probably different from the steps proposed for the pre-transition mechanism.

© 2005 Elsevier B.V. All rights reserved.

## 1. Introduction

Despite numerous works dedicated to the oxidation kinetics of zirconium alloys by pressurized water, water vapour or oxygen, the mechanisms and the rate-limiting steps for zirconia growth are not already established.

It is well-known that after a pseudo-parabolic first period [1–3], a kinetic transition occurs when the thick-

ness of the oxide layer exceeds a critical value, which corresponds to an increase in the oxidation rate, associated with the appearance of cracks and pores in the oxide layer [2,4,5].

In the post-transition stage, the oxidation curves are considered to be either linear [4] or to result from cyclic periods of increasing and decreasing rate [6].

In a previous work dedicated to the oxidation of Zircaloy-4 by water vapour [7], we have shown that great differences exist between the pre- and post-transition stages, from the kinetic point of view: before the transition, the oxidation rate is controlled by the diffusion of oxygen vacancies in the oxide layer, as usually suggested

\* Corresponding author. Tel.: +33 4 77 42 01 52; fax: +33 4 77 42 00 00.

E-mail address: [fvaldivieso@emse.fr](mailto:fvaldivieso@emse.fr) (F. Valdivieso).

in the literature data. On the contrary, in the post-transition stage, the assumption of the rate-limiting step is no more valid, so that the oxidation curves cannot be described by a succession of such diffusion-controlled periods.

As far as the oxidation of Nb-containing alloys is concerned, the shape of the kinetic curves (which give the weight gain versus time) is qualitatively similar to that obtained with Zircaloy. Nevertheless, Nb-containing alloys are oxidised faster than recrystallised Zircaloy in oxygen and in water vapour [4,8–12], at the beginning of the oxidation, but the kinetic transition is not so sharp in Nb-containing alloys and it occurs after a longer time. In autoclave, different results are obtained, these alloys showing in most cases a better resistance to corrosion [14,15].

Another difference between the two alloys is related to the effect of platinum on the oxidation rate: if platinum is deposited on the surface of an oxide layer grown on ZrNbO, in pre-transition, the oxidation rate increases, in oxygen [10] or in water vapour [11], whereas Pt has no effect on the oxidation of Zr4 [11,12].

In order to account for these results, the pre-transition stage of the oxidation of ZrNbO is suggested to be controlled by a mixed diffusion–reaction regime, and therefore in steady conditions [10,13].

Moreover, it has been shown that the oxidation rate depends on the niobium concentration in the zirconium alloy [16], which is interpreted by the authors by the assumption that the reduction of the proton at the surface of the zirconia layer is the rate-limiting step [16]. On the other hand, Bömhert [17] thinks that the growth of zirconia is controlled by the diffusion through the pores and grain boundaries in the porous outer layer. In this last work, the pre- and post-transition stages are not distinguished.

Taking into account the numerous points of view, the existence and the nature of a rate-limiting step is still a matter of interest.

Concerning the influence of the water vapour pressure on the oxidation rate, no article is devoted to this subject, to our knowledge.

Finally, due to the lack of consistent data on the effect of water vapour on the oxidation rate before and after the transition, and in order to confirm (or not) these interpretations, we have decided to study the oxidation of a Nb-containing zirconium alloy, ZrNbO alloy, at 530 °C, following the same methodology as in the case of Zircaloy-4 [7].

This methodology allows to verify experimentally the validity of the kinetic assumptions generally used to account for the experimental results:

- (i) the steady-state assumption (which is necessary to assume the existence of a rate-limiting step) can be verified by measuring the oxidation rate with two

techniques (for example, simultaneous thermogravimetry and calorimetry [7,18–20]: if the system proceeds in a steady-state, the rates of weight gain and the heat flow should remain proportional during all the reaction),

- (ii) the assumption of the rate-limiting step can be verified using a method based on jumps of temperature or pressure [7,18–21]. Usually, the rate of solid-state reactions is written as

$$\frac{d\alpha}{dt} = A \exp\left(-\frac{E}{RT}\right) f(\alpha), \quad (1)$$

where  $\alpha$  is the fractional conversion,  $A$  is the pre-exponential factor,  $E$  is the activation energy and  $f(\alpha)$  can take various expressions depending on the chosen model. Eq. (1) implies that the rate is controlled by a step following the Arrhenius law (which is not always verified, for example in the case of an interface rate-limiting step involving a gas adsorbed according to the Langmuir isotherm). Eq. (1) also implies that, at a given temperature, the rate is fixed by the value of  $\alpha$  (due to the function  $f(\alpha)$ ), which may not be the case, particularly when nucleation and growth processes are in competition.

We prefer a more general expression for the rate, given by Eq. (2)

$$\frac{d\alpha}{dt} = \Phi(T, P_i) \cdot E(t) \quad (2)$$

in which  $\Phi$  is a rate per unit area, it depends on the nature of the rate-limiting step (diffusion, interface reaction), it is independent on time but may be a function of temperature  $T$  and partial pressures of the reacting and/or produced gases  $P_i$ .  $E(t)$  is a function related to the extent of the reaction zone where the rate-limiting step is located. The interest of the general expression Eq. (2) is that it only assumes the existence of a rate-limiting step for the growth of the new phase, but no additional assumption is made concerning the nature and the localisation of this step.

Once the points (i) and (ii) have been validated experimentally, Eq. (2) can be used. Then the jump method also allows to obtain directly from experiments the variation of the  $\Phi$  function with  $T$  and  $P_i$ , which is very useful to find a growth mechanism and to identify the rate-limiting step.

Thus, the main aim of this article is to clearly put in evidence the differences that may exist between the pre- and post-transition stages in the case of the oxidation of ZrNbO by water vapour, and to answer to these questions:

- Does the oxidation of ZrNbO proceed in a steady-state in both stages?

- Is the assumption of a rate-limiting step justified in one (or both) stages?
- If there exists a rate-limiting step in one (or both) domains, what is the influence of the water pressure on the oxidation rate, and how can it be interpreted?

On the basis of the results of the kinetic study and sample characterisation (hydrogen pick-up ratio, scanning electron microscopy), different interpretations will be proposed for the pre- and post-transition kinetic behaviours.

## 2. Experimental

A 0.4 mm thick sheet of recrystallised ZrNbO alloy was used, and samples were cut to 10 × 10 mm for thermogravimetric experiments, and 15 × 15 mm for simultaneous thermogravimetry and calorimetry experiments. The alloy composition is indicated in Table 1. The sample surface was cleaned with an equimolar solution of ethanol and acetone in ultrasonic waves, then with pure ethanol and dried with compressed air.

The oxidation curves were obtained in isothermal and isobaric conditions at 500 and 530 °C with a symmetrical thermoanalyser SETARAM TAG16, under a flowing mixture of water vapour and hydrogen in helium. The flowrate of the gases was controlled by mass-flowmeters (Brooks 5850S), the total flowrate being 2.3 l h<sup>-1</sup>, and the partial pressure of hydrogen being usually equal to 10 h Pa. The water vapour partial pressure was fixed in the range 13–80 h Pa, using thermoregulated baths. It was controlled using humidity sensors (Transmicor 241–242 Coreci), placed at the inlet and outlet of the thermobalance furnace.

Jumps in hydrogen pressure were carried out by changing the flowmeter setpoint, whereas jumps in water vapour pressure were performed by switching the gaseous flow from one water bath to another one maintained at a different temperature.

The simultaneous thermogravimetry and calorimetry experiments were performed using a Setaram TG/DSC 111, under flowing mixtures of water vapour and hydrogen in helium.

The morphology of the oxide layers was observed by scanning electron microscopy (SEM DSM 960A Zeiss).

Table 1  
Composition of the ZrNbO alloy

Fe (ppm)	Nb (wt%)	O (ppm)
354	1.03	1303

## 3. Results

### 3.1. Shape of the oxidation curves

Fig. 1 represents a kinetic curve giving the mass gain per unit area  $m/S(t)$  versus time, and its derivative ( $d(m/S)/dt$ ), obtained at 530 °C (after an initial temperature rise of 30 °C/min from room temperature to 530 °C), under 10 h Pa in hydrogen and 13 h Pa in water vapour. The minimum of the rate corresponds to an oxide thickness (calculated from the weight gain) of about 10 μm. The curve appears to be approximately parabolic in the pre-transition stage, whereas the rate is constant after the transition.

### 3.2. Steady-state approximation

In Fig. 2, the variations of the rate of weight gain ( $dm/dt$ ) and the heat flow  $dQ/dt$  versus time are

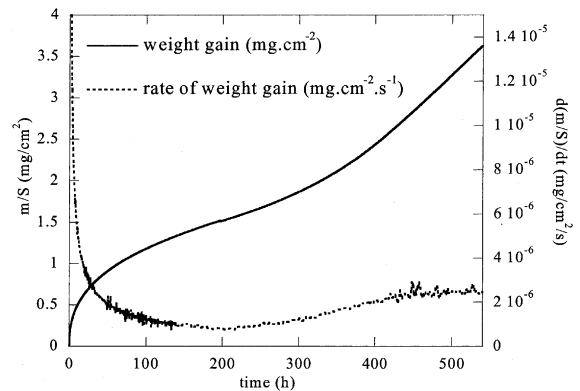


Fig. 1. Weight gain (—) and its derivative (---) versus time for ZrNbO at 530 °C in water vapour (13 h Pa) and hydrogen (10 h Pa), showing the pre- and post-transition stages.

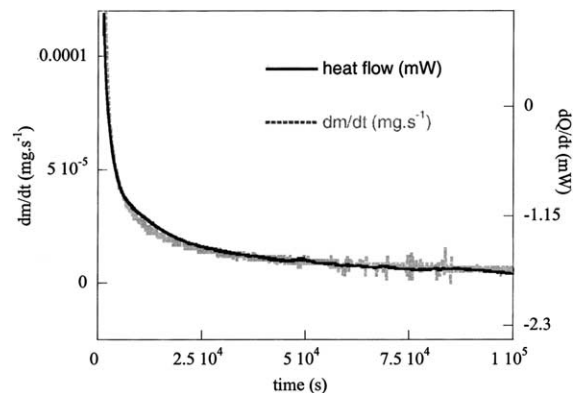


Fig. 2. Rate of weight gain (---  $dm/dt$ ) and heat flow (—) versus time for ZrNbO at 550 °C in water vapour (13 h Pa) and hydrogen (10 h Pa), for the pre-transition stage.

represented in the pre-transition stage, at 550 °C. A scaling factor allowing to superimpose the two curves could be found, which shows that the reacting system is in a steady-state before the transition.

Several experiments were performed up to the transition, confirming the results of Fig. 2. Unfortunately, only the very beginning of the transition was reached in TG/DSC experiments, the linear regime characteristic of the post-transition stage could not be reached, even for experiments lasting more than one month. Maybe the post-transition stage could have been observed in a higher pressure in water vapour, but it was not possible to increase the water vapour pressure in this thermogravimetric analyser.

Consequently, the steady-state approximation could not be verified after the transition.

### 3.3. Rate-limiting step assumption

When a rate-limiting step can be assumed, Eq. (2) gives the variations of the oxidation rate with the intensive variables ( $T, P_i, \dots$ ) and the time. In isobaric and isothermal conditions, the variations of the rate with time are given by  $E(t)$ ,  $\Phi(T, P_i)$  remaining constant. A sudden change (jump) in temperature or partial pressure during an experiment will then lead to a change in  $\Phi$ , while  $E(t)$  will be approximately constant (provided that the time necessary for the  $T$  or  $P$  change is short enough).

Thus the ratio of the rates measured after (at the right side) and before (at the left side) the jump is equal to  $\Phi_2/\Phi_1$  ( $E(t)$  being eliminated in the ratio).

Performing a series of similar jumps at various reaction times will lead to a series of  $\Phi_2/\Phi_1$  ratios, which must be identical if Eq. (2) can be applied.

This method, that we have named the ' $\Phi E$  test', has been successfully used in previous works [7,18–21]. The results are indicated on Fig. 3, for sudden changes in temperature from 500 to 530 °C ( $P_{\text{H}_2\text{O}} = 13$  h Pa,  $P_{\text{H}_2} = 10$  h Pa) in pre-transition stage (Fig. 3(a)), and from 530 to 500 °C in post-transition (Fig. 3(b)).

Since it takes a very long time to reach the post-transition stage, the post-transition samples have been preliminarily oxidised simultaneously at 530 °C up to an oxide thickness equal to 17  $\mu\text{m}$  (calculated from the weight gain), then each of them was submitted separately to a temperature change at a given time.

Considering the experimental errors bars, the ratio keeps a constant value ( $2.17 \pm 0.1$  for temperature jumps from 500 to 530 °C (Fig. 3(a)) and  $2.13 \pm 0.1$  for temperature jumps from 530 to 500 °C (Fig. 3(b))) during the pre-transition stage, up to about 6  $\mu\text{m}$ . Then the ratio decreases between 6  $\mu\text{m}$  and 12  $\mu\text{m}$ , during the transition, and becomes again constant after 17  $\mu\text{m}$ , in the post-transition stage (characterised by a linear regime with a constant rate).

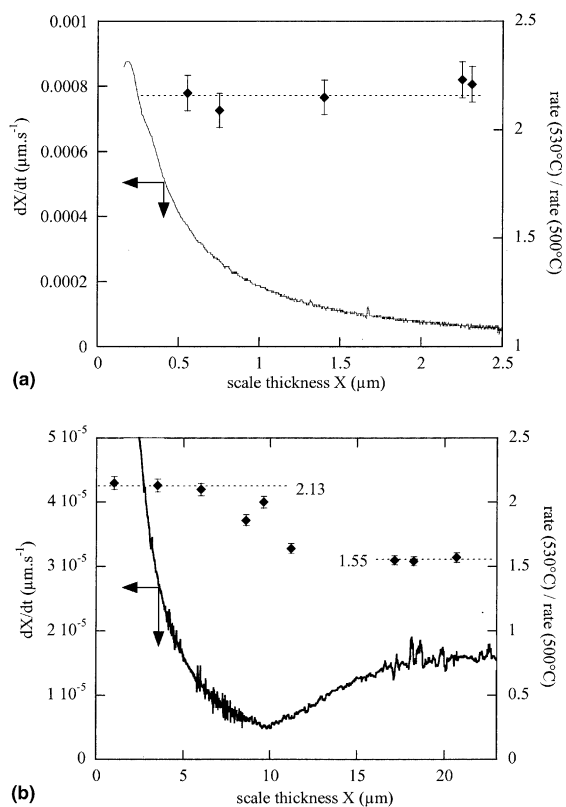


Fig. 3. Rate of weight gain (530 °C,  $P_{\text{H}_2\text{O}} = 13$  h Pa,  $P_{\text{H}_2} = 10$  h Pa) and ratios of the rate before and after the temperature jumps, in the pre- (a) and post-transition (b) stages.

Consequently, it can be concluded that:

- the ' $\Phi E$  test' is validated in the pre-transition domain; as the steady-state assumption is also verified, there exists a rate-limiting step in this stage. Moreover, it must be noticed that a mixed diffusion–reaction controlling rate is not in agreement with the results of the ' $\Phi E$  test', because in such a case the ratios of the rates would not be constant [11,20];
- the kinetic transition characterised by the decrease in the ratio of the rates begins at about 7  $\mu\text{m}$ , before the minimum in the oxidation rate, observed at about 10  $\mu\text{m}$  in Fig. 3(b);
- the ' $\Phi E$  test' is also verified in the post-transition stage, but the value of the ratio is clearly lower than its value in the pre-transition stage ( $1.55 \pm 0.08$  instead of  $2.13 \pm 0.1$ ). For the steady-state study, the oxidation time was not long enough to conclude on the state of the reaction system, but as the ' $\Phi E$  test' is validated, the assumption of a rate-limiting step can be made; besides, the linear shape of the kinetic curves in post-transition suggests that an interface step could be rate-limiting. Obviously, a

change in the rate-limiting step occurs between the pre- and post-transition stages, since the shape of the curves and the values of the rate ratios are different.

### 3.4. Influence of $H_2O$ and $H_2$ partial pressures

#### 3.4.1. Pre-transition stage

The variations of  $\Phi$  with a gas partial pressure  $P$  can easily be obtained by performing sudden changes, from  $P_0$  to  $P$ , at a given thickness  $X$ , the ratio of the rates being then equal to  $\Phi(P)/\Phi(P_0)$  [7,19,21]. The experiments were carried out at 500 °C, with 10 h Pa in hydrogen and a water vapour pressure varying from 13 h Pa ( $P_0$ ) to 80 h Pa after the jump. For the hydrogen pressure jumps, the water pressure was fixed at 13 h Pa and the hydrogen pressures changed from 10 h Pa ( $P_0$ ) to 40 h Pa.

The variations of  $\Phi$  with  $P_{H_2O}$  are represented on Fig. 4: the water vapour pressure has a slight accelerating effect.

On the contrary, the hydrogen pressure has no effect on the oxidation rate, as shown in Table 2.

#### 3.4.2. Post-transition stage

Jumps in water vapour pressure have been performed at an oxide thickness equal to 25  $\mu\text{m}$  (in the linear part

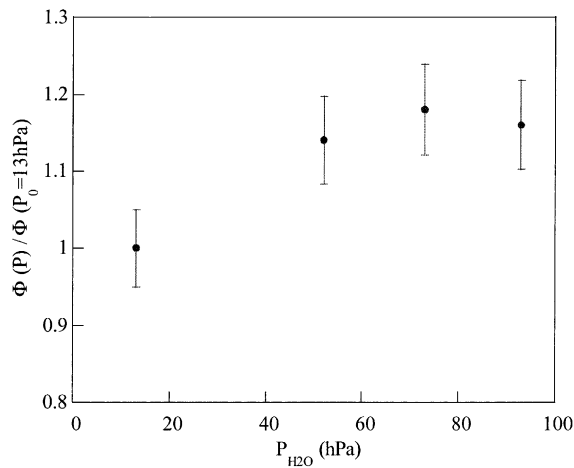


Fig. 4. Variations of the reactivity of growth  $\Phi$  with the partial pressure of water vapour, in the pre-transition stage (jumps from  $P_{H_2O} = 13$  h Pa to  $P$ , for  $X = 2.5$   $\mu\text{m}$ ,  $T = 500$  °C,  $P_{H_2} = 10$  h Pa).

Table 2

Ratios of the rates for jumps in hydrogen pressure from  $P_0 = 10$  h Pa to  $P$ , at a given thickness  $X = 2.6$   $\mu\text{m}$

$P_{H_2}$ (h Pa)	2	10	25	40
$dm/dt(P)/dm/dt(P_0)$	0.99	1	1.04	0.95

of the curves), from are 13 h Pa to 80 h Pa. The variations with  $P_{H_2O}$  of the ratio  $\Phi(P)/\Phi(P_0)$  are given in Fig. 5: the  $\Phi$  function increases with  $P_{H_2O}$ , the accelerating effect being more pronounced than in the pre-transition stage.

The ratio of the rates obtained from hydrogen pressure jumps, at a thickness  $X$  equal to 23  $\mu\text{m}$ , are reported in Table 3: as in the pre-transition stage, the hydrogen pressure has no effect on the oxidation rate.

### 3.5. Consequences of the results 3.1 to 3.4

The results obtained in Sections 3.1 to 3.4 have been summarized in Table 4. It can be concluded that the rate-limiting step approximation is verified in pre- and post-transition stages, but the rate-controlling steps are not the same before and after the transition. The  $\Phi$  function is different from one domain to another, which is in agreement with the change in the shape of the kinetic curves and in the sensitivity to water vapour pressure before and after the transition.

### 3.6. Effect of Nb content

An alloy containing 0.4 wt% in niobium (Zr0.4%NbO) has been used, in order to compare its

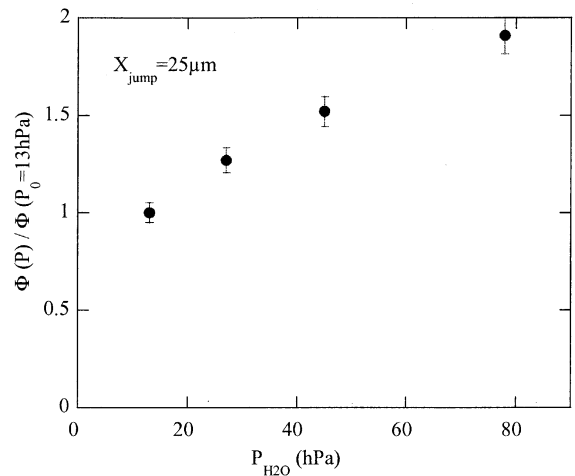


Fig. 5. Variations of the reactivity of growth  $\Phi$  with the partial pressure of water vapour, in the post-transition stage (jumps from  $P_{H_2O} = 13$  h Pa to  $P$ , for  $X = 25$   $\mu\text{m}$ ,  $T = 530$  °C,  $P_{H_2} = 10$  h Pa).

Table 3

Ratios of the rates for jumps in hydrogen pressure from  $P_0 = 10$  h Pa to  $P$ , at a given thickness  $X = 23$   $\mu\text{m}$

$P_{H_2}$ (h Pa)	2.5	10	22	40
$dm/dt(P)/dm/dt(P_0)$	0.98	1	1.01	1.07

Table 4  
Summary of kinetic results in pre- and post-transition stages

	Pre-transition	Post-transition
Steady-state	Yes	Not determined
$\Phi E$ test	Yes	Yes (after $X = 17 \mu\text{m}$ )
Rate-limiting step	Yes	Yes
H <sub>2</sub> O partial pressure	Slight accelerating effect	Accelerating effect (more pronounced than in pre-transition)
H <sub>2</sub> partial pressure	No effect	No effect

oxidation behaviour to ZrNbO one. Its composition is given in Table 5, this alloy does not contain  $\beta$ -Nb precipitates but contains Zr(Nb,Fe)<sub>2</sub> phases [22]. The oxidation curves giving the oxide thickness  $X$  versus time, obtained for the two alloys at 520 °C under 13 h Pa in hydrogen and 67 h Pa in water vapour are represented on Fig. 6. It can be seen that the higher the Nb content, the higher the oxidation rate in pre-transition (which is in agreement with the literature data) [16,23–25]. The post-transition stage was not reached, in the experiment, with Zr0.4%NbO alloy.

Fig. 7 shows the rate curves  $dX/dt$  versus  $X$  for both alloys. A scaling factor allowing to superimpose the two curves could be found, which means that the oxidation rates of these two alloys remain proportional during all the reaction time, with a ratio equal to 1.5. It is worth noticing that this ratio is lower than the ratio of the Nb concentration in the alloys (equal to 2.5).

Table 5  
Composition of the Zr0.4%NbO alloy

Nb (wt%)	Fe(ppm)	Cr(ppm)	O(ppm)
0.41	175	25	840

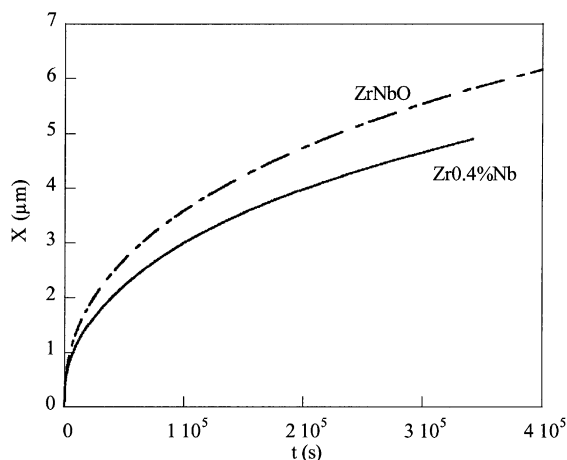


Fig. 6. Oxide thickness versus time for ZrNbO and Zr0.4%Nb ( $T = 520 \text{ }^\circ\text{C}$ ,  $P_{\text{H}_2\text{O}} = 13 \text{ h Pa}$ ,  $P_{\text{H}_2} = 10 \text{ h Pa}$ ).

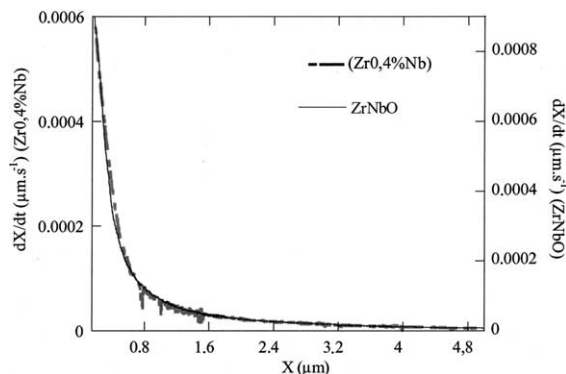


Fig. 7. Oxidation rate ( $dX/dt$ ) versus time for Zr0.4%Nb (dotted line) and ZrNbO (—).

### 3.7. SEM characterisation of the samples

The cross-sectional views of the oxide scale grown during the pre-transition stage present a continuous and uniform layer adherent to the substrate. Fig. 8(a) and (b) show micrographs of samples oxidised at 530 °C in 13 h Pa and 10 h Pa of water vapour and hydrogen respectively. The thickness calculated from the weight gain is 3.5  $\mu\text{m}$  for Fig. 8(a) and 6  $\mu\text{m}$  for Fig. 8(b). The metal/oxide interface is more or less undulated, and short cracks parallel to the interface appear regularly inside the layer [9]. A delayed oxidation can also be observed straight above some of these cracks.

Similar cracks are observed in samples oxidised after the kinetic transition, up to an oxide thickness of 12  $\mu\text{m}$  and more. Moreover, new large cracks are observed which are perpendicular to the metal/oxide interface and connected to the gaseous atmosphere.

## 4. Discussion

### 4.1. Pre-transition

Since the steady-state and the ' $\Phi E$  test' have been validated experimentally, the assumption of a rate-determining step can be made and the oxidation rate is given by ( $X$  is the oxide thickness)

$$\frac{dX}{dt} = \frac{V_{\text{ox}} n_0}{2S_0} \Phi(T, P_i) E(t), \quad (3)$$

where  $V_{\text{ox}}$  is the molar volume of the oxide ( $\text{m}^3 \text{mol}^{-1}$ ),  $n_0$  is the initial amount of metal (mol),  $S_0$  is the surface of the samples ( $\text{m}^2$ ).

It has been observed that the  $\Phi$  function increases with the partial pressure of water vapour. A simple mechanism involving oxygen vacancies can be written to describe zirconia growth [7], which provides a good interpretation of the oxidation of Zircaloy-4.



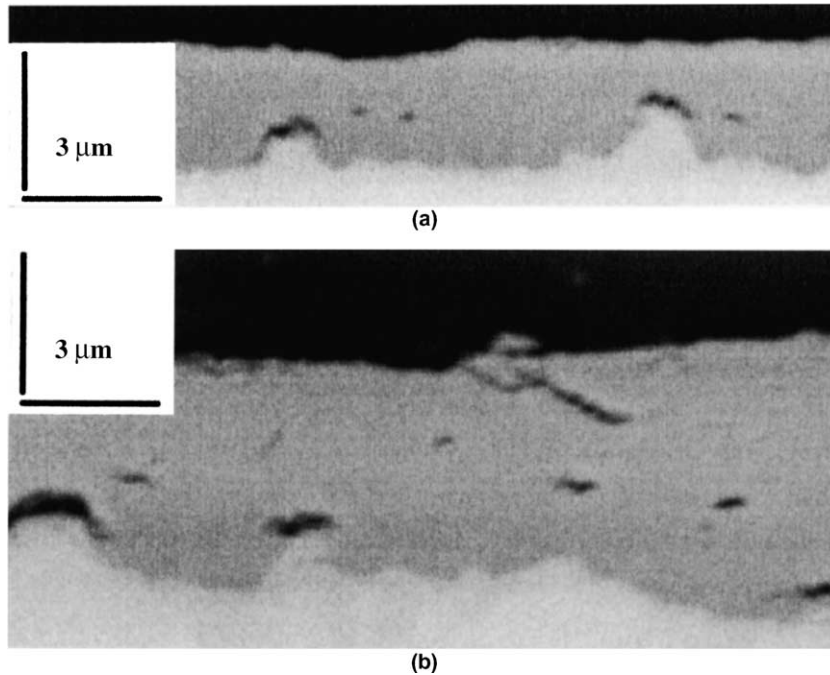


Fig. 8. Cross-sectional views of oxide layers grown on ZrNbO at 530 °C ( $P_{\text{H}_2\text{O}} = 13 \text{ h Pa}$ ,  $P_{\text{H}_2} = 10 \text{ h Pa}$ ):  $X \approx 3.5 \mu\text{m}$  (a) and  $X \approx 6 \mu\text{m}$  (b).

From this mechanism, it is well-known that only a rate-limiting step located at the external interface (gas/oxide) can account for an accelerating effect of the partial pressure on the  $\Phi$  function, this rate-limiting step being either the water adsorption step, the interface reaction step or the hydrogen desorption step.

If such an interface step was rate-limiting, the oxidation rate should be constant with time and the kinetic curves should be linear, which is not the case.

Some authors [10,13] have interpreted the curves with a mixed reaction–diffusion rate, but in that case it can be shown that the ‘ $\Phi E$  test’ would not be validated, since the expression of the rate would be [20]

$$\frac{dX}{dt} = \frac{n_0 V_{\text{ox}}}{2S_0} \frac{1}{\frac{1}{\Phi_{\text{diffusion}}(T, P_i) E_{\text{diffusion}}(t)} + \frac{1}{\Phi_{\text{interface}}(T, P_i) S_0}} \quad (4)$$

Thus this assumption is not in agreement with our experimental results.

Consequently, a new mechanism has to be proposed to describe zirconia growth on ZrNbO alloy. What kind of elementary steps should be considered to explain the influence of the water vapour partial pressure and the decreasing rate? The dissociation of water vapour at the surface of the oxide probably leads to the formation of adsorbed hydroxyl groups (OH) and then, the diffu-

sion of such species through the oxide layer may predominate. Considering the SEM micrographs of our samples (Fig. 8(a) and (b)), the oxide layer appears to be homogeneous (excepted a few cracks). Nevertheless, it has been found by impedance spectroscopy [10,26] that the oxide layer grown on ZrNbO could be divided into two sub-layers. For the kinetic modelling, two possibilities can be imagined, involving one or two oxide layers:

- either one oxide layer with micropores and diffusion of adsorbed species via this porosity,
- or two oxide layers: the microporous layer and a very thin and dense layer near the metal/oxide interface (for example, the native oxide layer), in which the diffusion of oxygen vacancies is very rapid. The thickness of this dense layer is assumed to remain very small during all the pre-transition stage.

In both cases, the weight gain is considered to be due only to the growth of the microporous oxide layer. The oxygen transport through this layer is supposed to occur via adsorbed hydroxyl groups (as seen in the mechanism below); thus, a part of the hydrogen produced by the oxidation is released near the metal/oxide interface. Adsorbed hydrogen can migrate through the micropores towards the external interface.

The various steps involved in the growth mechanism are detailed below:

- External interface (gas/oxide)
  - (1) adsorption of water on adsorption sites  $s$   
 $H_2O + s \rightleftharpoons H_2O - s$
  - (2) dissociation of water into OH groups  
 $H_2O - s + s \rightleftharpoons OH - s + H - s$
  - (3) reduction of hydroxyl groups  
 $OH - s + e' \rightleftharpoons OH^- - s$
  - (4) desorption of hydrogen  
 $2H - s \rightleftharpoons H_2 + 2s$
  - (5) diffusion of adsorbed OH groups in the porous layer.
- Intermediate interface (porous layer/dense layer)
  - (6) interface step  
 $OH^- - s + V_0^{**} + e' \rightleftharpoons H - s + O_0$
  - (7) hydrogen desorption at the intermediate interface  
 $2H - s \rightleftharpoons H_2 + 2s$
  - (8) diffusion of oxygen in the dense layer.
- Internal interface
  - (9) internal interface step  
 $Zr_{\text{alloy}} \rightleftharpoons Zr_{Zr(\text{ox})} + 2V_0^{**} + 4e'$

The hydrogen amount in the metal can be neglected in the total weight gain (this is in agreement with the very low amount of hydrogen measured by Cezus in the metal in the pre-transition stage (about 30 ppm)).

In order to account for the decrease in the rate versus time in pre-transition, we have to consider a diffusion step as rate-limiting. The kinetic curves being not strictly parabolic, we have successfully fitted them using the following equation (as previously done in our study of Zircaloy-4 oxidation [7]):

$$\frac{dX}{dt} = \frac{k_1}{X} \exp(-k_2X) \quad (5)$$

in which  $X$  represents the thickness of the microporous layer.

To our knowledge, two distinct models can lead to Eq. (5): first, the existence of barriers for the diffusing species in the oxide layer (such as pores or cracks), randomly distributed [27,28]; secondly, the effect of a gradient of compressive stress [29,30], under some approximations. The expression of  $k_2$  depends on the physical modelling, but in both cases  $k_1$  is equal to:  $V_{\text{ox}}DC$ , where  $D$  is the coefficient of diffusion of the diffusing species,  $C$  is its concentration at the interface of departure (neglecting the concentration of the diffusing species at the interface of arrival).

The curves giving the rate  $dX/dt$  versus  $X$  were fitted using several laws (parabolic, cubic, power . . .), the com-

parison of these fits are given in Fig. 9. Eq. (5) always leads to the best agreement with all our experiments.

From Eq. (5), by comparison to Eq. (3), the  $\Phi(T, P_i)$  and  $E(t)$  functions can be easily calculated

$$\phi(T, P_i) = \frac{D \cdot C}{X_0}, \quad (6)$$

$$E(t) = \frac{D \cdot CS_0 X_0 \exp(-k_2 X)}{n_0 X}, \quad (7)$$

$X_0$  is a characteristic length, for example the initial thickness of the sample. The variations with temperature and partial pressures of the  $\Phi(T, P_i)$  function are deduced from the growth mechanism detailed above. Assuming that the rate-limiting step is the diffusion of adsorbed hydroxyl groups  $OH^- - s$  from the external interface into the porous layer via the surface of the pores, and neglecting the concentration of  $OH^- - s$  groups at the interface of arrival, the  $\Phi$  function can be calculated

$$\Phi(T, P_i) = \frac{D}{X_0} \theta_0 \times \frac{K_1 K_2 K_3 \beta P_{H_2O}}{P_{H_2O} \left( K_1 K_2 (1 + K_3 \beta) + K_1 \sqrt{\frac{P_{H_2}}{K_4}} \right) + \sqrt{\frac{P_{H_2}}{K_4}} + \frac{P_{H_2}}{K_4}} \quad (8)$$

in which  $K_i$  is the equilibrium constant of the step ( $i$ ),  $\theta_0$  is the concentration of adsorption sites per unit of surface area, and  $\beta$  is the electrons activity in the oxide layer, which is supposed to be fixed by the Nb content in solid solution in the oxide

$$[e'] = [Nb_{Zr}^*] = \beta. \quad (9)$$

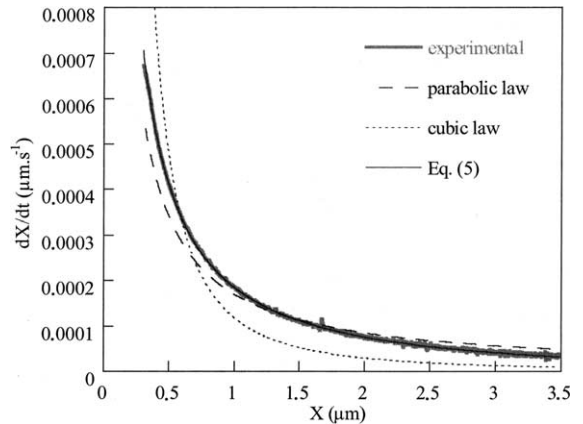


Fig. 9. Rate of oxidation of ZrNbO as a function of the oxide thickness before the kinetic transition – comparison with various rate laws.



The variations of  $\Phi(T, P_i)$  with  $P_{\text{H}_2\text{O}}$  follow an hyperbolic law, according to

$$\Phi(T, P_{\text{H}_2\text{O}}) = \frac{P_{\text{H}_2\text{O}}}{1 + qP_{\text{H}_2\text{O}}}, \quad (10)$$

where

$$q = \frac{K_1 K_2 (1 + K_3 \beta) + \sqrt{\frac{P_{\text{H}_2}}{K_4}} K_1}{\sqrt{\frac{P_{\text{H}_2}}{K_4}} + \frac{P_{\text{H}_2}}{K_4}}. \quad (11)$$

This law is in good agreement with the experimental data, as shown in Fig. 10. The fit leads to a value of  $q$  equal to 0.38.

From Eq. (8),  $\Phi(P)$  should vary with hydrogen pressure like  $\frac{1}{a+bP_{\text{H}_2}+c\sqrt{P_{\text{H}_2}}}$ , but no influence of  $P_{\text{H}_2}$  was observed experimentally in the range (2.5–40 hPa). Thus, Eq. (8) is not in agreement with our experimental results. However, this law exhibits a constant behaviour when  $P_{\text{H}_2}$  increases, so experiments at lower hydrogen pressure would have been useful to validate it. Moreover, Eq. (8) shows that if the value of the equilibrium constant  $K_4$  is high compared to the values of  $P_{\text{H}_2}$ , the term  $P_{\text{H}_2}/K_4$  may become very small and may be neglected besides the other terms. In that case, no effect of hydrogen pressure would be observed on the oxidation rate. Unfortunately, information on the values of the various equilibrium constants are not available in order to support one of these suggestions. The  $\Phi(T, P_i)$  function depends on the Nb content in solid solution in the oxide,  $\beta$ , according to an hyperbolic law  $A\beta/(1+B\beta)$ . Experiments have shown that an increase in the Nb content of the alloy increases the oxidation rate, and the oxidation rates of ZrNbO and Zr0.4%Nb are proportional, in a ratio equal to 1.5.

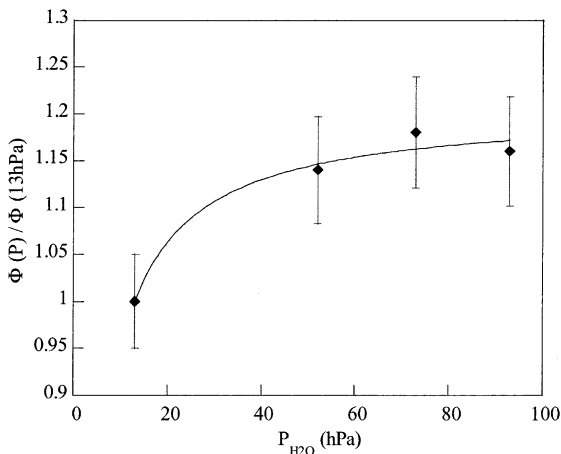


Fig. 10. Variations of the reactivity of growth  $\Phi$  with the partial pressure of water vapour: experimental data ( $\blacklozenge$ ) and calculated law (continuous line), in the pre-transition stage.

The Nb content in solid solution in the alloys is about 0.37% for ZrNbO [22] and 0.27% in Zr0.4%Nb. The Nb content in solution in the oxide layer,  $\beta$ , being unknown, if we use the previous values (Nb content of the alloys), we can calculate the value of  $B$  (in  $A\beta/(1+B\beta)$ ) which would give a ratio between  $\Phi(\text{ZrNbO})$  and  $\Phi(\text{Zr0.4\%Nb})$  equal to 1.5. This value is found to be negative, but becomes positive if the Nb content in the oxide,  $\beta(\text{ZrNbO})$ , is increased from 0.37% to 0.4%. This small variation is within the error range on the measurements, but it could also mean that the amount of Nb dissolved in the oxide is not exactly equal to the amount initially dissolved in the alloy. Thus, concerning the influence of Nb content, the predictions of the model are in agreement with our experimental results.

It has also been observed that platinum has an accelerating effect on the oxidation rate of ZrNbO [10,11], in water vapour or oxygen. The electrons supplied by the platinum layer would be involved in step (3) of the mechanism described above. Due to the noble metal on the oxide surface, the electrochemical potential of the electrons, which corresponds to the energy of the Fermi level, is increased at this interface, since the energy of the Fermi level is higher for a metal than for a semi-conductor [31]. Besides, the equilibrium constant  $K_3$  depends on the electrochemical potential of the electrons, it increases if the electrons potential increases. Consequently, the platinum layer leads to an increase of the equilibrium constant  $K_3$ . In that case, Eq. (8) shows that the oxidation rate is increased. Consequently, this model allows to propose an interpretation of the effect of platinum on the oxidation rate of ZrNbO.

Finally, we have shown that the pre-transition stage in ZrNbO oxidation cannot be accounted for by the mechanism usually proposed for the oxidation of zirconium alloys, which involves the diffusion of oxygen vacancies through the dense oxide layer as the rate controlling step. Thus, we have proposed another mechanism allowing to account for the accelerating effect of water vapour and Nb content. The important feature is to demonstrate that it is possible to explain the influence of the gases without assuming necessarily an interface rate-limiting step. In the case of ZrNbO, the oxidation is assumed to be controlled by a diffusion step, in which the concentration gradient of the diffusing species is fixed by a step located at the external interface (and not by a step located at the metal/oxide interface, as in the mechanism proposed usually).

#### 4.2. Transition and post-transition

It is clear from the results of the jumps method (Figs. 3(b) and 5) that the diffusion step controlling the beginning of the oxidation is no longer valid, even before the rate reaches its lowest value (since the ratios of the rates obtained with the jumps method decreases from about

7 μm, whereas the oxidation rate is minimum at about 10 μm, see Fig. 3(b)). Large cracks connecting a part of the oxide layer to the gaseous atmosphere appear from this point, which could be related to the increase in the rate after the transition.

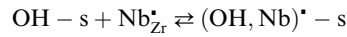
Then, when the oxide thickness exceeds 17 μm, the shape of the kinetic curve is linear. Moreover, the ratio of the rates remains constant (with a value different from the pre-transition one, see Fig. 3(b)). Consequently, it can be deduced that the post-transition stage is controlled by an interface step, largely influenced by the water vapour pressure. Another possibility could be the diffusion through a layer with a constant thickness, but this is less probable due to the influence of the water vapour pressure.

Now, what could be the mechanism and the rate-controlling step in this stage? If the same mechanism as in the pre-transition stage can be considered, the expressions of the rate calculated assuming that the rate-controlling step is located at the external interface (steps 2, 3 or 4) are reported in Table 6: these three laws are in agreement with the effect of water vapour (cf. Fig. 5).

However, Fig. 3(b) shows that, when the oxide thickness is lower than 5 μm, the rate in pre-transition stage (controlled by the diffusion of hydroxyl groups) is higher than the rate observed in post-transition. Thus, if the rates of the various steps involved in the growth mechanism are nearly the same in pre- and post-transition stages, the interface step controlling the post-transition rate cannot be a step belonging to the mechanism proposed for the pre-transition stage.

On the contrary, the pre-transition mechanism could explain the post-transition kinetics if the rate of one of the interface steps of this mechanism became far lower in post-transition than it was in pre-transition. A possi-

ble reason for such a change in the rate of an interface step could be a change in the concentrations of the point defects of the oxide involved in the mechanism: for example, we may imagine the formation of associated defects such as (OH, Nb) according to



Such defects would lead to a decrease in the concentration of OH-s species, and consequently in a decrease in the rate of step (3). Other point defects could probably be considered.

Another way to explain the post-transition kinetics would be a change in the mechanism, involving completely different steps.

Unfortunately, we have no experimental evidence to support one of these suggestions. More investigations would be necessary to give a valuable interpretation of the post-transition kinetics.

## 5. Conclusion

The oxidation of a ZrNbO alloy in a mixture of hydrogen and water vapour at 530 °C exhibits clear differences between the pre- and post-transition stages.

In pre-transition, the oxidation proceeds in a steady-state, and is influenced by water vapour and Nb content, whereas hydrogen pressure has no effect in the studied range. The rate decreases with time, according to a sub-parabolic law.

A mechanism has been proposed to account for these results, which involves the diffusion of adsorbed OH groups in a microporous part of the oxide layer, as rate-determining step.

Table 6  
Expressions of the rate laws corresponding to the rate-controlling steps (2)–(4)

Rate-limiting step	Growth reactivity $\Phi$
Step (2)	$\Phi(T, P_i) = \frac{k_2 K_1 P_{\text{H}_2\text{O}}}{\left(1 + K_1 P_{\text{H}_2\text{O}} + \sqrt{\frac{P_{\text{H}_2}}{K_4}} \left(1 + \frac{\sqrt{K_4}}{K_3 K_6 \sqrt{K_4 K_9}} + \frac{\sqrt{K_4} \beta}{K_6 \sqrt{K_7 K_9}}\right)\right)^2}$
Step (3)	$\Phi(T, P_i) = \frac{k_3 K_1 K_2 \sqrt{K_4} \beta P_{\text{H}_2\text{O}}}{P_{\text{H}_2\text{O}} (K_1 \sqrt{P_{\text{H}_2}} + K_1 K_2 \sqrt{K_4}) + \sqrt{P_{\text{H}_2}} + P_{\text{H}_2} \left(1 + \frac{1}{\sqrt{K_4}} + \frac{\beta}{K_6 \sqrt{K_7 K_9}}\right)}$
Step (4)	$\Phi(T, P_i) = \frac{k_4 (K_1 K_2 K_3 K_6 \sqrt{K_7 K_9})^2 P_{\text{H}_2\text{O}}^2}{P_{\text{H}_2} \left(1 + P_{\text{H}_2\text{O}} \left(K_1 + \frac{K_1 K_2 K_3 K_6 \sqrt{K_7 K_9}}{\sqrt{P_{\text{H}_2}}}\right) + \frac{\sqrt{P_{\text{H}_2}}}{K_6 \sqrt{K_7 K_9}} + \left(\beta + \frac{1}{K_3}\right)\right)^2}$

$k_i$  and  $K_i$  are respectively the rate constant and the equilibrium constant of the step ( $i$ ).

Then, after a transition period beginning at about 7  $\mu\text{m}$  at 530  $^{\circ}\text{C}$ , a rate-limiting step can again be considered when the oxide thickness is higher than 17  $\mu\text{m}$ . As the curves are linear, the oxidation is probably controlled by an interface step. This step has not been determined, but it is probably different from the steps proposed in the pre-transition mechanism.

Consequently, the transition is accompanied by a change in the oxidation mechanism, that could be linked to the change in the morphology of the oxide layer.

### Acknowledgments

This work has been carried out with the financial support of FRAMATOME-ANP. We would like to thank P. Barberis (Cezus) and A. Frichet (Framatome-ANP) for helpful discussions.

### References

- [1] H.A. Porte, J.G. Schnizlein, R.C. Vogel, D.F. Fisher, J. Electrochem. Soc. 107 (1960) 506.
- [2] J.K. Dawson, G. Long, W.E. Seddon, J.F. White, J. Nucl. Mater. 25 (1968) 179.
- [3] T. Arima, K. Moriyam, N. Gaja, H. Furuya, K. Idemitsu, Y. Inagaki, J. Nucl. Mater. 257 (1998) 67.
- [4] B. Cox, J. Nucl. Mater. 148 (1987) 332.
- [5] J.J. Kearns, J. Nucl. Mater. 22 (1967) 292.
- [6] M. Parise, Thesis, Paris, 1996.
- [7] M. Tupin, M. Pijolat, F. Valdivieso, M. Soustelle, A. Frichet, P. Barberis, J. Nucl. Mater. 317 (2003) 130.
- [8] N. Petigny, P. Barberis, C. Lemaignan, C. Valot, M. Lallemand, J. Nucl. Mater. 280 (2000) 318.
- [9] P. Bossis, Thesis, Grenoble, 1999.
- [10] J.J. Vermoyal, A. Frichet, L. Dessemond, J. Nucl. Mater. 328 (2004) 31.
- [11] M. Tupin, Thesis, Saint-Etienne, 2002.
- [12] J.J. Vermoyal, L. Dessemond, A. Hammou, A. Frichet, J. Nucl. Mater. 298 (2001) 297.
- [13] A. Frichet, P. Barberis, N. Petigny, in: 12th Symposium on Zirconium in the Nuclear Industry, Toronto, 15–18 June 1998.
- [14] G.P. Sabol, G.R. Kilp, M.G. Balfour, E. Roberts, in: Zirconium in the nuclear industry, 8th international symposium, ASTM STP 1023 (1989) 227.
- [15] J.P. Mardon, D. Charquet, J. Senevat, in: Proceedings of the International Meeting on Light Water Reactor Fuel Performance, West Pam Beach, Florida, 17–21 April 1994, p. 643.
- [16] K.N. Choo, S. Pyun, Y. Kim, J. Nucl. Mater. 226 (1995) 9.
- [17] J. Böhmert, M. Dietrich, J. Linek, Nucl. Eng. Des. 147 (1993) 53.
- [18] K. Surla, F. Valdivieso, M. Pijolat, M. Soustelle, M. Prin, Ann. Chim. Sci. Mater. 25 (2000) 601.
- [19] K. Surla, F. Valdivieso, M. Pijolat, M. Soustelle, M. Prin, Solid State Ion. 143 (2001) 355.
- [20] F. Ledoux, F. Valdivieso, M. Pijolat, M. Soustelle, A. Frichet, P. Barberis, Mater. Sci. Forum 369–372 (1) (2001) 223.
- [21] K. Nahdi, S. Perrin, M. Pijolat, F. Rouquerol, N. Ariguib, M. Ayadi, Phys. Chem. Chem. Phys. 4 (2002) 1972.
- [22] P. Barberis, D. Charquet, V. Rebeyrolle, J. Nucl. Mater. 326 (2004) 163.
- [23] H.H. Klepfer, J. Nucl. Mater. 9 (1963) 65.
- [24] Y.H. Jeong, H.G. Kim, D.J. Kim, B.K. Choi, J.H. Kim, J. Nucl. Mater. 323 (2003) 72.
- [25] H.G. Kim, Y.H. Jeong, T.H. Kim, J. Nucl. Mater. 326 (2004) 125.
- [26] F. Garzarolli, H. Seidel, R. Tricot, J.P. Gros, in: Zirconium in the nuclear industry, 9th international symposium, ASTM STP 1132 (1991) 395.
- [27] U.R. Evans, in: Proceedings of the Ninety-first General Meeting at Louisville, Ky, 12 April 1947, p. 547.
- [28] M. Cournil, G. Thomas, J. Chim. Phys. 74 (1977) 545.
- [29] G.A. Eloff, C.J. Greyling, P.E. Viljoen, J. Nucl. Mater. 199 (1993) 285.
- [30] C.C. Dollins, M. Jursich, J. Nucl. Mater. 113 (1983) 19.
- [31] C. Deportes et al., Electrochimie Des Solides, EDP Sciences, 1994.